Journal of Alloys and Compounds 713 (2017) 156–163

Contents lists available at ScienceDirect

Journal of Alloys and Compounds

journal homepage: http://www.elsevier.com/locate/jalcom

Microwave synthesis and spectroscopic properties of ternary scheelite-type molybdate phosphors $NaSrLa(MoO_4)_3:Er^{3+},Yb^{3+}$

Chang Sung Lim [a], Aleksandr S. Aleksandrovsky [b, c], Maxim S. Molokeev [d, e, f], Aleksandr S. Oreshonkov [g, h], Victor V. Atuchin [i, j, k, l, m, *]

[a] Department of Advanced Materials Science & Engineering, Hanseo University, Seosan 356-706, Republic of Korea
[b] Laboratory of Coherent Optics, Kirensky Institute of Physics, Federal Research Center KSC SB RAS, Krasnoyarsk 660036, Russia
[c] Laboratory for Nonlinear Optics and Spectroscopy, Siberian Federal University, Krasnoyarsk 660041, Russia
[d] Laboratory of Crystal Physics, Kirensky Institute of Physics, Federal Research Center KSC SB RAS, Krasnoyarsk 660036, Russia
[e] Department of Physics, Far Eastern State Transport University, Khabarovsk 680021, Russia
[f] Institute of Engineering Physics and Radioelectronics, Siberian State University, Krasnoyarsk 660074, Russia
[g] Laboratory of Molecular Spectroscopy, Kirensky Institute of Physics, Federal Research Center KSC SB RAS, Krasnoyarsk 660036, Russia
[h] Department of Photonics and Laser Technologies, Siberian Federal University, Krasnoyarsk 660079, Russia
[i] Laboratory of Optical Materials and Structures, Institute of Semiconductor Physics, SB RAS, Novosibirsk 630090, Russia
[j] Functional Electronics Laboratory, Tomsk State University, Tomsk 634050, Russia
[k] Laboratory of Semiconductor and Dielectric Materials, Novosibirsk State University, Novosibirsk 630090, Russia
[l] Institute of Chemistry, Tyumen State University, Tyumen 625003, Russia
[m] Laboratory of Single Crystal Growth, South Ural State University, Chelyabinsk 454080, Russia

ARTICLE INFO

Article history:
Received 6 March 2017
Received in revised form
4 April 2017
Accepted 6 April 2017
Available online 7 April 2017

Keywords:
Microwave synthesis
Crystal structure
Molybdate phosphor
Frequency up conversion

ABSTRACT

Ternary scheelite-type molybdate $NaSrLa_{(1-x-y)}(MoO_4)_3:xEr^{3+},yYb^{3+}$ ($x = y = 0$, $x = 0.1$ and $y = 0.2$, $x = 0.05$ and $y = 0.45$, $x = 0.2$ and $y = 0$) phosphors were successfully synthesized by the microwave sol-gel method for the first time. Well-crystallized particles formed after the heat-treatment at 900 °C for 16 h showed a fine and homogeneous morphology with a particle size of 2–3 μm. The crystal structures were refined by the Rietveld method in space group $I4_1/a$. The optical properties were examined comparatively using photoluminescence emission and Raman spectroscopy. Under the excitation at 980 nm, the $NaSrLa_{0.7}(MoO_4)_3:0.1Er^{3+},0.2Yb^{3+}$ and $NaSrLa_{0.5}(MoO_4)_3:0.05Er^{3+},0.45Yb^{3+}$ particles exhibited a strong 525-nm emission band, a weaker 550-nm emission band in the green region and weak 655-nm, 490-nm and 410-nm emission bands in the red, blue and violet regions. The pump power dependence and Commission Internationale de L'Eclairage chromaticity of the upconversion emission intensity were evaluated in detail. The presence of Sr in $NaSrLa(MoO_4)_3$, in comparison with $NaCaLa(MoO_4)_3$ compound, leads to frequency shift mainly in the low region of Raman spectra. The MoO_4 bending vibrations are most susceptible to changes in the distance between the nearest oxygen atoms in the nearest neighboring MoO_4 groups.

© 2017 Elsevier B.V. All rights reserved.

1. Introduction

The rare-earth-doped upconversion (UC) materials possess specific luminescent properties and they show their potential for applications in such photonic structures as solar cells, displays and biological tissue imaging [1–3]. The spectroscopic and chemical characteristics of the UC materials, in many aspects, defined by the host parameters and complex oxide hosts are among the best because of their pronounced chemical and mechanical stability under ambient conditions, appropriate synthesis technologies and structural diversity [4–10]. Earlier, the binary rare-earth-containing scheelite-structure-related molybdates were successfully synthesized and their structural and optical properties were obtained in detail, including the phenomenon of structure modulation and UC photoluminescence [7,10–15]. Among the known compounds, binary molybdates $NaLn(MoO_4)_2$ (Ln = La^{3+}, Ce^{3+}, Gd^{3+}, Y^{3+}, Bi^{3+}) possess the tetragonal structure in space group $I4_1/a$ [12,16,17]. In these and similar structures, the constituent

* Corresponding author. Institute of Semiconductor Physics, SB RAS, Novosibirsk 630090, Russia.
E-mail address: atuchin@isp.nsc.ru (V.V. Atuchin).

http://dx.doi.org/10.1016/j.jallcom.2017.04.060
0925-8388/© 2017 Elsevier B.V. All rights reserved.

trivalent elements can be efficiently substituted by Er^{3+}, Ho^{3+}, Tm^{3+} or Yb^{3+} and other rare-earth ions commonly used in the UC and wLED media [10–15,18–22]. The rare earth ions can be incorporated into the crystal lattice of the tetragonal binary molybdates with a low defect generation due to the similarity of trivalent rare earth ion radii, and the solid solution phosphors show high photoluminescence efficiency [10,13–15,21–25].

Among rare-earth elements, the pair of Er^{3+}/Yb^{3+} is very suitable for the frequency conversion from the infrared to visible range via the UC process due to its appropriate energy level configurations. Indeed, the Yb^{3+} ion, taken as a sensitizer, can be efficiently excited by the infrared LED source at λ ~800 nm. Then, this energy can be transferred to the Er^{3+} activator from which the visible range radiation can be emitted. In the UC medium, Er^{3+} ions are the luminescence centers and the Yb^{3+} sensitizer enhances the UC efficiency. It was shown earlier that the Er^{3+}/Yb^{3+} co-doping can remarkably enhance the UC efficiency for the shift from the infrared (λ ~ 800 nm) to green light due to the proficient energy transfer from Yb^{3+} to Er^{3+} [26–29]. Nevertheless, it is topical to create new ternary molybdate crystalline hosts for the observation of the UC photoluminescence in the materials and search for such critical parameters as the well-defined particle morphology and stable UC luminescent properties. However, only one ternary molybdate from the $NaRLn(MoO_4)_3$ (R = Ca^{2+}, Sr^{2+} and Ba^{2+}, and Ln are rare-earth elements) family and one closely related tungstate $NaSrLa(WO_4)_3$ have been discovered up to now [30,31] and a further research is needed to reveal the potential of the molybdate hosts.

As compared to the commonly used technological methods, microwave synthesis provides such advantages as a very short reaction time, small and uniform particle size and high purity of the final polycrystalline product [32,33]. It is a cost-effective method that provides high homogeneity powder products and it is easy to scale-up the process up to the industrial level. Thus, the microwave method is considered as a viable alternative technology for the quick synthesis of high-quality luminescent materials. In this concept, the method seems be optimal for the synthesis of complex oxide compounds. In the present study, the ternary molybdate $NaSrLa_{1-x-y}(MoO_4)_3$:$x$$Er^{3+}$,$y$$Yb^{3+}$ (NSLM:$x$$Er^{3+}$,$y$$Yb^{3+}$) phosphors with the selected doping concentrations were successfully prepared by the microwave sol-gel method followed by high-temperature calcination in the air. The evaluated compositions can be found in Table 1. The synthesized particles were characterized by X-ray diffraction (XRD) and scanning electron microscopy (SEM). The spectroscopic properties were examined comparatively using Raman spectroscopy and photoluminescence (PL) emission. The pump power dependence and Commission Internationale de L'Eclairage (CIE) chromaticity parameters of the UC emission were evaluated in detail.

2. Experimental

In this experiment, the stoichiometric amounts of $Na_2MoO_4 \cdot 2H_2O$ (99%, Sigma-Aldrich, USA), $Sr(NO_3)_3 \cdot 4H_2O$ (99%, Sigma-Aldrich, USA), $La(NO_3)_3 \cdot 6H_2O$ (99%, Sigma-Aldrich, USA), $(NH_4)_6Mo_7O_{24} \cdot 4H_2O$ (99%, Alfa Aesar, USA), $Er(NO_3)_3 \cdot 5H_2O$ (99.9%, Sigma-Aldrich, USA), $Yb(NO_3)_3 \cdot 5H_2O$ (99.9%, Sigma-Aldrich, USA), citric acid (99.5%, Daejung Chemicals, Korea), $NH_3 \cdot H_2O$ (A.R.), ethylene glycol (A.R.) and distilled water were used to synthesize the compositions $NaSrLa(MoO_4)_3$, $NaSrLa_{0.8}(MoO_4)_3$:$0.2Er^{3+}$, $NaSrLa_{0.7}(MoO_4)_3$:$0.1Er^{3+}$,$0.2Yb^{3+}$ and $NaSrLa_{0.50}(MoO_4)_3$:$0.05Er^{3+}$,$0.45Yb^{3+}$. To prepare the compounds, initially, $Sr(NO_3)_3 \cdot 4H_2O$, $Na_2MoO_4 \cdot 2H_2O$ and $(NH_4)_6Mo_7O_{24} \cdot 4H_2O$ were dissolved in 20 mL of ethylene glycol and 80 mL of 5 M $NH_3 \cdot H_2O$ under vigorous stirring and heating. Subsequently, $La(NO_3)_3 \cdot 6H_2O$ with $Er(NO_3)_3 \cdot 5H_2O$, $Yb(NO_3)_3 \cdot 5H_2O$ and citric acid (with the molar ratio of citric acid to the total metal ions of 2:1) were dissolved in 100 mL of distilled water. The reagents were taken in accordance to the nominal composition of the designed compounds. Then, the solutions were mixed together vigorously and heated at 80–100 °C. Finally, highly transparent solutions were obtained and adjusted to pH = 7–8 by the addition of $NH_3 \cdot H_2O$ or citric acid. The solutions were placed into a microwave oven operating at the frequency of 2.45 GHz with the maximum output-power of 1250 W for 30 min. The working cycle of the microwave reaction was precisely controlled using the regime of 40 s on and 20 s off for 15 min; this was followed by a further treatment of 30 s on and 30 s off for 15 min. The samples were treated with ultrasonic radiation for 10 min to produce a light yellowish transparent sol. After this, the sols were dried at 120 °C in a dry oven to obtain black dried gels. The black dried gels were ground and preheated at 350 °C for 12 h to evaporate the remained ethylene glycol and substantial organic compounds. Continuously, the clean particles without impurities were heat-treated at 900 °C for 16 h at 100 °C intervals between 600 and 900 °C. Finally, white particles were obtained for pure $NaSrLa(MoO_4)_3$, and light yellowish-pink particles were obtained for the doped compositions.

The powder diffraction measurements of the synthesized samples for the Rietveld analysis were collected over the angle range of 2θ = 5–90° with a D/MAX 2200 (Rigaku, Japan) diffractometer (Cu-Kα radiation, θ-2θ geometry) at room temperature. The step size of 2θ was 0.02°, and the counting time was 2 s per step. The surface morphology and microstructure of the powder particles were observed using SEM (JSM-5600, JEOL, Japan). The PL spectra were recorded using a spectrophotometer (Perkin Elmer LS55, UK) at room temperature. The dependence of the UC emission intensity on the pump power was measured at working power levels 20–110 mW. Raman spectra measurements were performed using

Table 1
Main parameters of processing and refinement of the $NaSrLa_{1-x-y}MoO_4$:xEr,yYb samples.

Compound	x, y	Space group	Z	Cell parameters (Å), cell volume (Å^3)	R_p, R_B (%) χ^2
NSLM	0, 0	$I4_1/a$	4	a = 5.3603 (1) c = 11.8274 (3) V = 339.84 (2)	13.83, 6.60 1.25
NSLM: 0.2Er	0.2, 0	$I4_1/a$	4	a = 5.3406 (1) c = 11.7769 (2) V = 335.90 (2)	12.08, 4.11 1.16
NSLM: 0.1Er,0.2Yb	0.1, 0.2	$I4_1/a$	4	a = 5.3293 (1) c = 11.7479 (3) V = 333.65 (2)	10.39, 2.34 1.14
NSLM: 0.05Er,0.45Yb	0.05, 0.45	$I4_1/a$	4	a = 5.3063 (1) c = 11.6820 (3) V = 328.92 (1)	9.61, 2.62 1.11

a LabRam Aramis (Horiba Jobin-Yvon, France) at the spectral resolution of 2 cm^{-1}. The 514.5-nm line of an Ar ion laser was used as an excitation source and, to avoid the sample decomposition, the power on the sample surface was kept at a level below 0.5 mW.

3. Results and discussion

The XRD patterns recorded from the synthesized molybdates are shown in Fig. 1 and Figs. S1-S3. As it is evident from comparison, the patterns of the NSLM:xEr^{3+},yYb^{3+} compounds are very similar and they can be described by the same type of the structure. There is no indication of any foreign crystalline phase. As an example, the difference profile plot of NSLM is shown in Fig. 1. For other samples, the difference profile plots can be observed in Supporting Information (Figs. S1-S3). The Rietveld refinement for each compound was performed using a TOPAS 4.2 package [34]. All diffraction peaks were indexed by the tetragonal unit cell in space group $I4_1/a$ with parameters close to those of $CaMoO_4$ [35] and $Na_{0.5}La_{0.5}MoO_4$ [36]. The $Na_{0.5}La_{0.5}MoO_4$ scheelite was taken as a reference because this molybdate and NSLM contain Na^+ and La^{3+} ions. Therefore, these crystal structures were selected as the starting model for the Rietveld refinement. A site of the Sr or (Na/La) ion was taken as occupied by Sr, Na, La, Er, Yb ions at fixed occupations according to the nominal compositions. The refinements were stable and gave low R-factors (Table 1, Fig. S1-S3). The obtained coordinates of atoms and the main bond lengths are reported on in Tables S1 and S2, respectively. The linear cell volume increases on the averaged increase of ion radii IR(Na/Sr/La/Er/Yb), as shown in Fig. 2, and this proves the chemical compositions of the synthesized samples [37]. The crystal structure of $NaSrLa(MoO_4)_3$-based solid solution crystals is depicted in Fig. 3. Generally, the structure is analogous to that of $CaMoO_4$ [35]. Further details of the crystal structures may be obtained from Fachinformationszentrum Karlsruhe, 76344 Eggenstein-Leopoldshafen, Germany (fax: (+49) 7247-808-666; E-mail: crystdata@fiz-karlsruhe.de; http://www.fiz-karlsruhe.de/request_for_deposited_data.html on quoting the deposition numbers CSD-432334-432337. Thus, the high-temperature treatment at 900 °C in the air plays the crucial role in the molybdate gel crystallization and oxygen content restoration. As it can be reasonably assumed, high temperatures close to 900 °C are optimal for molybdate treatment in the air and, previously, many simple and complex molybdates were crystallized at similar temperatures [7,11,15,22,27,30,38–42].

It is interesting to consider the behavior of unit cell volume in scheelite type molybdate solid solutions as a function of cation radii. As it could be assumed on the base of the dependence found for the $NaSrLa(MoO_4)_3$-based solid solutions, as shown in Fig. 3, other complex molybdates crystallized in a scheelite structure

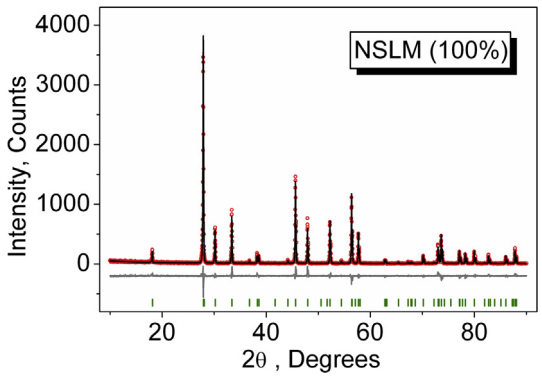

Fig. 1. Difference Rietveld plot of $NaSrLa(MoO_4)_3$.

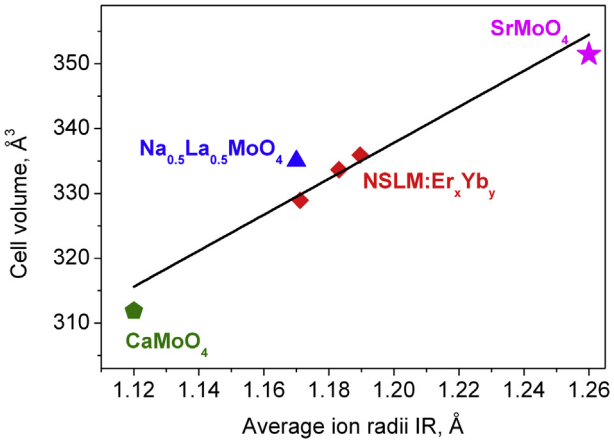

Fig. 2. Cell volume per averaged ion radii IR(Na/Sr/La/Er/Yb) of $CaMoO_4$ (green pentagon) [37], $Na_{0.5}La_{0.5}MoO_4$ (blue triangle) [38], $SrMoO_4$ (purple star) compounds. (For interpretation of the references to colour in this figure legend, the reader is referred to the web version of this article.)

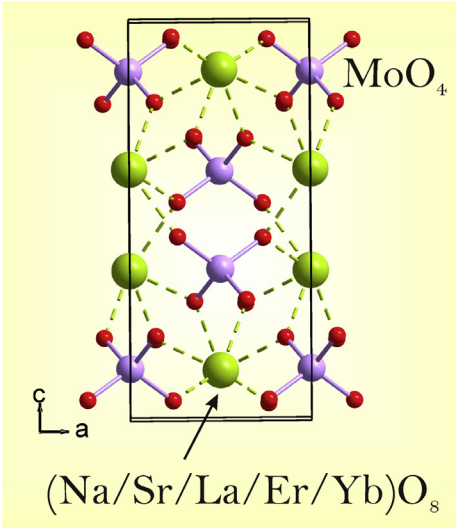

Fig. 3. The crystal structure of $NaSrLa(MoO_4)_3$-based solid solutions. The lone atoms are omitted for clarity.

should also follow this trend. However, real situation is found to be more complex. The dependences of unit cell volume on average ion radii (IR), except for Mo^{6+}, for several scheelite type molybdates containing rare earth, alkaline and Ag^+ ions are shown in Fig. 4. The related structural data used for the calculations can be found elsewhere [16,24,36,37,43–63]. In molybdates $Li_{0.5}Ln_{0.5}MoO_4$, $K_{0.5}Ln_{0.5}MoO_4$, $Ag_{0.5}Ln_{0.5}MoO_4$ and $Na(Ca,Sr)Ln(MoO_4)_3$, the cell volume is proportional to the average IR value. However, for each metal from the set of M = Li, Na, K and Ag, the curve is individual. As it can be reasonably supposed, the type of M^+ cation in the crystal composition governs the position of the molybdate family at this diagram. This is a specific empirical rule for complex molybdates with the scheelite type structure. As it is well known, the scheelite structure is very stable and, in this structure, even the presence of structural vacancy is acceptable when it is necessary to reach the charge neutrality of the lattice. Earlier, in several binary molybdates containing M metals, the existence of the structural vacancy was reported on [64–66]. The diagram shown in Fig. 4 opens the possibility for the vacancy size estimation in the $A_xLn_y\square_{1-x-y}MoO_4$

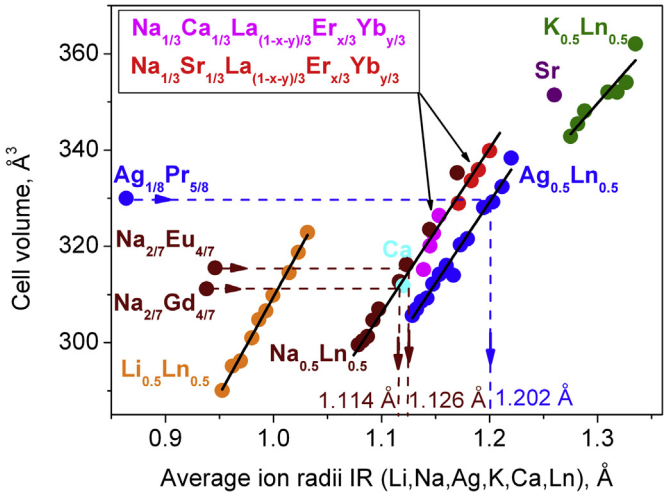

Fig. 4. Cell volume per average ion radii IR(Li,Na,Ag,K,Ca,Ln) in several scheelite-type molybdates families. The points of $CaMoO_4$ (Ca) and $SrMoO_4$ (Sr) are added for comparison. The dashed lines with arrows show the algorithm of estimation of average ion radii IR(Na,Ag,Ln) for the crystals with structural vacancies: $Na_{2/7}Gd_{4/71/7}MoO_4$, $Na_{2/7}Eu_{4/71/7}MoO_4$, $Ag_{1/8}Pr_{5/81/4}MoO_4$.

$(x + y < 1$, A = Li, Na, K) compounds. Indeed, $Na_{2/7}Gd_{4/7}\square_{1/7}MoO_4$ [65], which forms an incommensurate modulated crystal structure with space group *I*-4(α-β0,βα0)00 due to vacancies, has the big cell volume $V = 311.18$ Å^3, as calculated from the unit cell parameters [65]. This molybdate with structural vacancies is characterized by the very small average ion radii calculated using formal relation IR($Na_{2/7}Gd_{4/7}\square_{1/7}$, CN = 8) = 2/7•IR($Na^+$) + 4/7•IR($Gd^{3+}$) = 0.938 Å [67]. Thus, in Fig. 4, the point related to molybdate $Na_{2/7}Gd_{4/7}\square_{1/7}MoO_4$ lies drastically away from the general curve obtained for M = Na. Comparatively, molybdate $Na_{0.5}Er_{0.5}MoO_4$ is without a structural vacancy and has a smaller cell volume (V = 303.07 Å^3), but much bigger calculated average ion radii IR($Na_{0.5}Er_{0.5}$) = 1.092 Å. The point related to $Na_{0.5}Er_{0.5}MoO_4$ lies at the general curve M = Na in Fig. 4. Then, if to suppose that all sheelite-type molybdates with M = Na should be governed by the general dependence obtained for Na-containing crystals, true average ion radii IR($Na_{2/7}Gd_{4/7}\square_{1/7}$, CN = 8) = 1.114 Å can be estimated, as shown in Fig. 4. It gave us the opportunity to calculate the average radii of vacancy IR(□, CN = 8) = 1.226 Å in $Na_{2/7}Gd_{4/7}\square_{1/7}MoO_4$ from the corrected relation IR($Na_{2/7}Gd_{4/7}\square_{1/7}$, CN = 8) = 2/7•IR($Na^+$) + 4/7•IR($Gd^{3+}$) + 1/7IR(□) = 1.114 Å. It is interesting that the structural vacancy size is much bigger than IR(Gd, CN = 8) = 1.053 and IR(Na, CN = 8) = 1.18 Å [67]. Similar calculations made for $Na_{2/7}Eu_{4/7}MoO_4$ [66] gave the close value of ion radii IR(□, CN = 8) = 1.258 Å. Averaging these values led to the value of IR(□, CN = 8) = 1.25(2) Å. The calculation of the vacancy ion radii for $Ag_{1/8}Pr_{5/8}\square_{2/8}MoO_4$ [64] using the same algorithm and Vegard law for M = Ag compounds, as shown in Fig. 4, gave even the bigger value IR(□, CN = 8) = 1.353 Å. Commonly, it can be assumed that the structural vacancy size increases in parallel with the cell volume increase. As far as the cell volume of compounds $M_{0.5}Ln_{0.5}MoO_4$ increases in the sequence of M = Li, Na, Ag, K (Fig. 4), the smallest vacancy size for $Li_xLn_y\square_zMoO_4$ and the biggest vacancy size for $K_xLn_y\square_zMoO_4$ can be reasonably expected.

The microwave synthesis followed by high temperature annealing in the air provides a very uniform closely agglomerated particle morphology, as it is evident from Fig. 5 where the SEM image of the synthesized NSLM particles is shown. The morphology of the samples containing Er and Yb is practically the same and they are not shown. The NSLM powder is formed by coalescent particles,

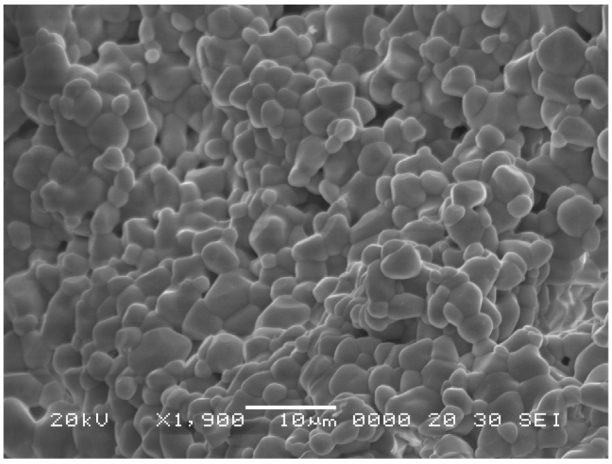

Fig. 5. A scanning electron microscopy image of the synthesized $NaSrLa(MoO_4)_3$ particles.

2–3 μm in size. As it was obtained previously in oxides, the closely agglomerated particles are commonly induced by the active interdiffusion of the grains that, as a rule, provides excellent composition homogeneity [4,10,25,68,69]. Thus, the fine particles with controlled morphology and high crystallinity can be fabricated by the microwave sol-gel route in a short time. The method is cost-effective and it can be easy scaled up and that is very promising for rapid synthesis of UC phosphors. This suggests that the microwave sol-gel route is suitable for the creation of homogeneous NSLM:xEr^{3+},yYb^{3+} crystallites and it can be successfully applied to other molybdates from this crystal family.

The upconversion properties of NSLM:xEr^{3+},yYb^{3+} solid solutions were investigated under the excitation at the wavelength 980 nm. The visible luminescence spectra of pure NSLM and three activated samples, namely, $NaSrLa(MoO_4)_3$, $NaSrLa_{0.8}(MoO_4)_3$:0.2Er^{3+}, $NaSrLa_{0.7}(MoO_4)_3$:0.1Er^{3+},0.2Yb^{3+} and $NaSrLa_{0.50}(MoO_4)_3$:0.05Er^{3+},0.45Yb^{3+} are presented in Fig. 6. The undoped NSLM, as must be expected for a defect-free crystal, shows no detectable luminescence in the visible range. In all three erbium-containing samples, the maximal luminescence is detected at erbium ion transitions from $^2H_{11/2}$ and $^4S_{3/2}$ states to the $^4I_{15/2}$ ground state, the first transition being dominant. The luminescence from $^4F_{9/2}$ is also present, but it is much weaker, indicating that

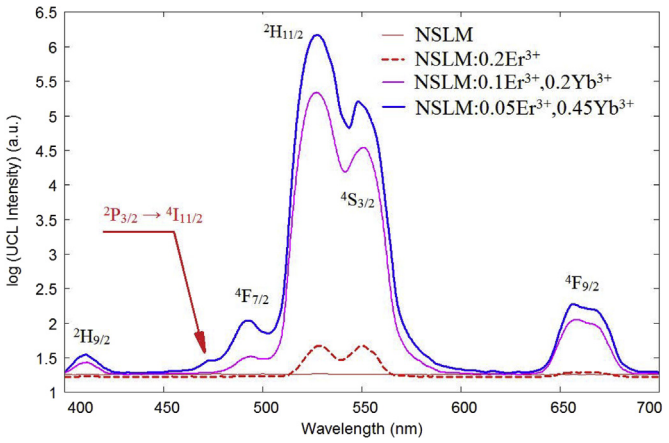

Fig. 6. The upconversion photoluminescence emission spectra of NSLM:Er,Yb particles excited at wavelength 980 nm at room temperature. The starting levels for UCL band terminating in the ground state are indicated in black.

prevailing upconversion population process terminates mainly at the $^2H_{11/2}$ level, while the relaxation from this level to $^4F_{9/2}$ is rather weak, like in other studied molybdates. Other detected upconversion luminescence bands are due to the transitions from $^2H_{9/2}$ (411 nm) and $^4F_{7/2}$ (493 nm). Generally, the spectral distribution of UCL in the NSLM matrix is close to that in recently studied $NaCaLa(MoO_4)_3:Er^{3+},Yb^{3+}$ [70]. Two differences can be noted: namely, a larger increase of $^4F_{7/2}$ luminescence when the Yb content reaches 45% and the appearance of an additional band at 474 nm and that is distinctly observable in this single sample with the highest Yb content. Erbium does not possess the energy level that can produce this additional band at the transition to the ground state. Hence, this additional band must be ascribed to the transition between excited states $^2P_{3/2} \rightarrow {}^4I_{11/2}$. This feature indicates a stronger energy transfer to high-lying Er levels in the NSLM matrix with Yb doping as high as 45%. The log-to-log dependence of three main upconversion luminescence bands of Er ion in NSLM doped with 45% of Yb are presented in Fig. 7. The slopes for green, yellow-green and red bands are correspondingly 1.7, 1.68 and 1.56, indicating a two-step population scheme of the starting levels of these bands. These slope values are completely identical to the case of Er ion upconversion obtained in the Yb-doped NCLM matrix.

The calculated chromaticity coordinates of (a) $NSLM:0.1Er^{3+},0.2Yb^{3+}$ and (b) $NSLM:0.05Er^{3+},0.45Yb^{3+}$ phosphors and the related CIE chromaticity diagram are shown in Fig. 8. The legend in Fig. 8(B) shows the chromaticity points for samples (a) and (b). When the Er^{3+}/Yb^{3+} concentration ratio is varied, the chromaticity coordinate values (x, y) are slightly changed. As shown in Fig. 8(A), the points with chromaticity coordinates x = 0.240 and y = 0.614 for (a) $NSLM:0.1Er^{3+},0.2Yb^{3+}$ and x = 0.242 and y = 0.643 for (b) $NSLM:0.05Er^{3+},0.45Yb^{3+}$ fall to the yellowish-green sector in the CIE diagram.

The group theory analysis predicts 17 Raman-active modes for the $NaSrLaMoO_4$ compound with a tetragonal unit cell in the space group $I4_1/a$ structure. These modes are distributed among the irreducible representations as 3Ag + 7Bg + 7Eg. Among these modes, 3 are symmetric stretching vibrations and 4 are bending vibrations of MoO_4 tetrahedra. The remaining modes belong to translational motions of big cation vibrations, librations and translations of tetrahedral groups.

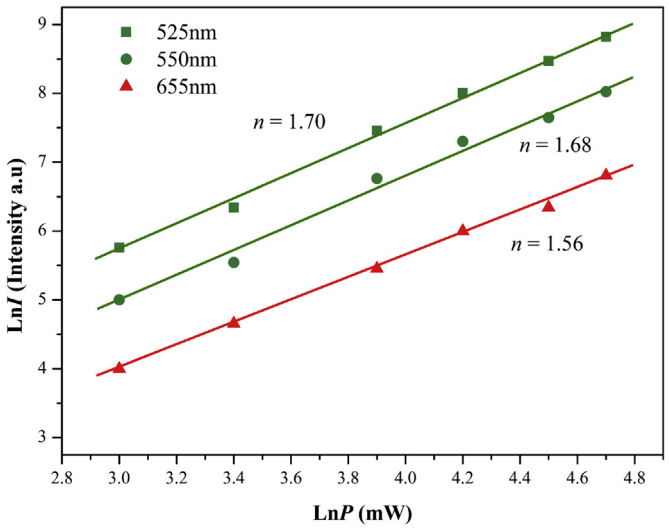

Fig. 7. The logarithmic scale dependence of the upconversion emission intensity on the pump power in the range from 20 to 110 mW at 545 and 655 nm in the $NaSrLa_{0.50}(MoO_4)_3:0.05Er^{3+},0.45Yb^{3+}$ sample.

The Raman spectra of the $NSLM:0.2Er^{3+}$, $NSLM:0.1Er^{3+},0.2Yb^{3+}$ and $NSLM:0.05Er^{3+},0.45Yb^3$ samples obtained under the 514.5 nm excitation at ambient conditions are shown in Fig. 9(a). Besides Raman lines, only Er^{3+} luminescent peaks can be seen in the spectra and, in the following, the features were excluded from the analysis. The Raman spectrum of NSLM is shown in Fig. 9(b) in comparison with the Raman spectrum of $NaCaLaM(MoO_4)_3$ (NCLM) [70]. As it can be seen from Fig. 9(b), the slight shift of the Raman peaks of NSLM in reference to those of NCLM is found. The obtained experimental values of Raman-active frequencies are presented in Table 2.

In order to assign the Raman peaks to the atom vibrations, we performed the lattice dynamics calculations of the Raman-active mode frequencies using the program package LADY [71]. The calculation algorithm and initial model parameters were the same as those used for the NCLM [70]. To find the model parameters, the special optimization program was written and tested for several compounds selected from different chemical classes [25,42,70,72–84]. The parameters obtained via the optimization are enumerated in Table S3. The most intense band in the Raman spectrum of NSLM is related to the ν_1 symmetric stretching vibration of the MoO_4 tetrahedral group [85]. The frequency shift of this line, in reference to that if NCLM, is mainly due to the Mo–O bond length difference, namely, 1.747 Å in NSLM and 1.77 Å in NCLM [70]. According to the empirical formula proposed in Ref. [86], $\nu(cm^{-1}) = 32895 \exp(-2.073\ R)$, where R is the bond distance in angstroms, the estimated frequency of ν_1 vibrations in NSLM should be 880 cm^{-1}, that is in good agreement with the experimental data, and this value should be bigger than that for NCLM where the Mo–O bond length is larger. The lines at 829 and 777 cm^{-1} are related to the ν_3 antisymmetric stretching vibrations. The bending ν_2 and ν_4 vibrations are positioned in the wavenumber region of 300–400 cm^{-1}. Generally, the frequency of ν_4 vibration should be higher than that of the ν_2 vibration [85]. The experimental data obtained for NSLM and NCLM, as well as our calculated results, are in agreement with this relation. Using frequency differentiation procedure [71], we can obtain the derivatives of calculated frequencies with respect to the potential model parameters. The results of the calculations indicate that the shift in the $_4$ vibration frequencies of NSLM and NCLM is related also to the difference in the distance between the nearest oxygen atoms of two nearest neighboring MoO_4 groups, 2.8900 and 2.8486 Å for NSLM and NCLM, correspondingly. Nevertheless, the influence of the difference between NSL–O and NCL–O bond lengths cannot be omitted. According to the above-presented, the ν_4 vibration frequencies of NCLM should be higher than these for NSLM that is in accordance with our experimental data. According to the lattice dynamics simulation, the Raman peaks in the region of 190 cm^{-1} correspond to the mode that comprises the coupled Na translation and libration of MoO_4 groups [86,87], and the difference in the position of experimental lines in NCLM and NSLM is mainly related to the difference in Na–O bond lengths. The same explanation is for the shift of the Raman line in the region about 140 cm^{-1}.

4. Conclusions

In the present work, the ternary molybdate $NSLM:xEr^{3+},yYb^{3+}$ phosphors were successfully synthesized by the microwave sol-gel method. The well-crystallized particles formed after heat-treatment at 900 °C for 16 h in the air showed a fine and homogeneous morphology with a characteristic particle size of 2–3 μm. The scheelite-type structures of pure NSLM and doped compositions were first defined by the Rietveld analysis. The new empirical rule for complex molybdates with general formula $M_xLn_yMoO_4$ (M = Li, Na, Ag, K) and the scheelite type structure was found. As it

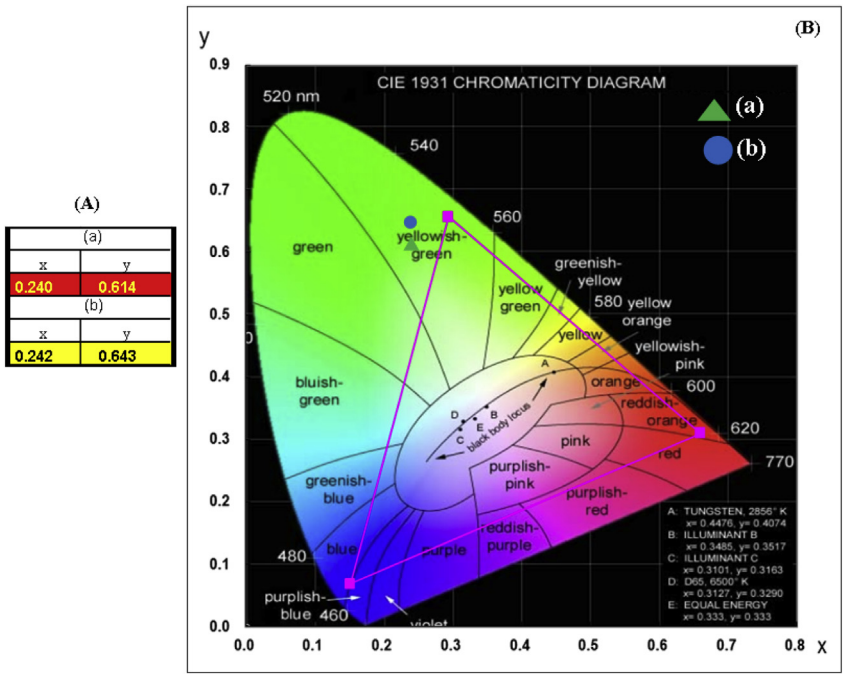

Fig. 8. (A) Calculated chromaticity coordinates (x, y) values and (B) the CIE chromaticity diagram for $NaSrLa_{1-x-y}(MoO_4)_3:xEr^{3+},yYb^{3+}$ phosphors. The emission points for samples (a) $NaSrLa_{0.7}(MoO_4)_3:Er_{0.1}Yb_{0.2}$ and (b) $NaSrLa_{0.50}(MoO_4)_3:Er_{0.05}Yb_{0.45}$ are shown in the inset.

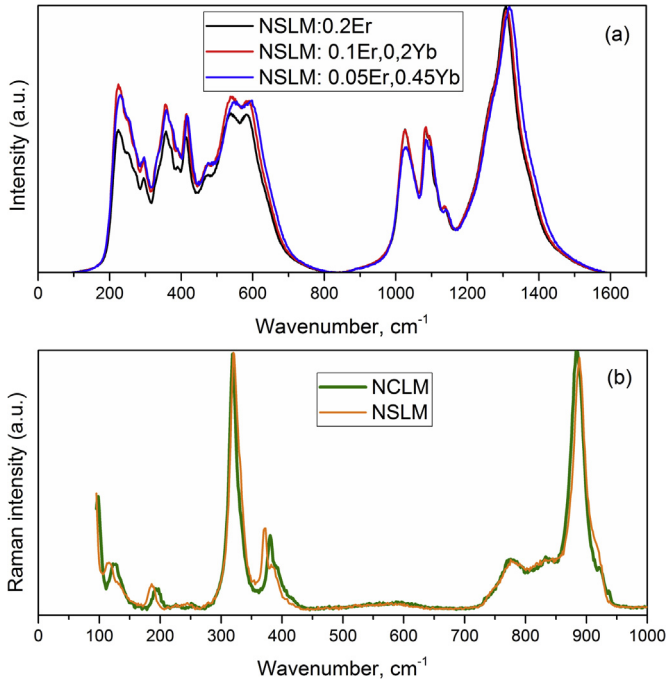

Fig. 9. The Raman spectra of synthesized $NaSrLa_{0.8}(MoO_4)_3:0.2Er^{3+}$, $NaSrLa_{0.7}(MoO_4)_3:0.1Er^{3+},0.2Yb^{3+}$, $NaSrLa_{0.50}(MoO_4)_3:0.05Er^{3+},0.45Yb^{3+}$ and pure $NaSrLa(MoO_4)_3$ in comparison with NCLM [70].

Table 2
Notation and wavenumber values (cm^{-1}) of the active Raman lines.

Number	Symm. type	calc		exp
		NSLM		NCLM [70]
1	A_g	881	888	885
2	B_g	817	829	829
3	E_g	793	777	777
4	B_g	383	386	390
5	E_g	360	371	380
6	B_g	324	332	332
7	A_g	346	320	318
8	E_g	256	244	255
9	B_g	220	224	228
10	A_g	176		195
11	E_g	185	186	190
12	Eg	130	136	141
13	B_g	118	114	125
14	B_g	97		
15	E_g	87		
16	B_g	21		
17	E_g	19		

was shown by a wide comparative observation, the type of M^+ cation governs the position of the selected molybdate family at the diagram where the cell volume is depicted as a function of average big ion radii IR(M_xLn_y). The compounds under investigation $Na_{1/3}Sr_{1/3}La_{(1-x-y)/3}MoO_4:x/3Er^{3+},y/3Yb^{3+}$ and the previously observed compounds $Na_{1/3}Ca_{1/3}La_{(1-x-y)/3}MoO_4:x/3Er^{3+},y/3Yb^{3+}$ revealed that the addition of a new element A = Ca, Sr to the formula $M_x(Ln,A)_yMoO_4$ does not lead to the appearance of new curve family *V*(IR), and the family is defined by the M^+ cation type. Such interesting property allowed us to suggest that the cell volume curve family of $M_xLn_y\square_zMoO_4$ compounds are also governed by M^+ cation only and this opens a way to estimate the radii of vacancy □ for several compounds: IR(□, CN = 8) = 1.226 Å in $Na_{2/7}Gd_{4/7}\square_{1/7}MoO_4$; IR(□, CN = 8) = 1.258 Å for $Na_{2/7}Eu_{4/7}\square_{1/7}MoO_4$; IR(□, CN = 8) = 1.353 Å for $Ag_{1/8}Pr_{5/8}\square_{2/8}MoO_4$. Two general trends were found: 1) vacancy size increases with an increase of the M^+ ion size, i.e. the vacancy size increases in parallel with the cell volume increase; 2) the structural vacancy size is much bigger than IR(Ln, CN = 8).

The upconversion luminescence of NSLM:Er,Yb under the 980 nm excitation is found to be generally similar to that of the recently investigated NCLM:Er,Yb, It is featured by the domination

of green luminescence from $^2H_{11/2}$ and by a low intensity of red luminescence. However, the NSLM:Er,Yb system at the Yb content of the order of 0.45 is found more favorable for the excitation of high-lying Er states, as indicated by the detection of UCL at 474 nm.

Acknowledgements

This research was supported by the Basic Science Research Program through the National Research Foundation of Korea (NRF) funded by the Ministry of Education (2016-944122) and by Project № 0356-2015-0412 of SB RAS Program №II.2P. The reported study was funded by RFBR according to the research project 16-52-48010 and 17-52-53031. Also, the work was supported by Act 211 Government of the Russian Federation, contract 02.A03.21.0011 and by the Ministry of Education and Science of the Russian Federation (4.1346.2017/PP).

Appendix A. Supplementary data

Supplementary data related to this article can be found at http://dx.doi.org/10.1016/j.jallcom.2017.04.060.

References

[1] Jing Zhou, Qian Liu, Wei Feng, Yun Sun, Fuyou Li, Upconversion luminescent materials: advances and applications, Chem. Rev. 115 (1) (2015) 395–465.
[2] Wei Zheng, Ping Huang, Datao Tu, En Ma, Haomiao Zhu, Xueyuan Chen, Lanthanide-doped upconversion nano-bioprobes: electronic structures, optical properties, and biodetection, Chem. Soc. Rev. 44 (2015) 1379–1415.
[3] Bo Zhou, Bingyang Shi, Dayong Jin, Xiaogang Liu, Controlling upconversion nanocrystals for emerging applications, Nat. Nanotechnol. 10 (11) (2015) 924–936.
[4] V.V. Atuchin, T.A. Gavrilova, J.-C. Grivel, V.G. Kesler, Electronic structure of layered ferroelectric high-k titanate $La_2Ti_2O_7$, J. Phys. D. Appl. Phys. 42 (2009) 035305.
[5] A.S. Aleksandrovsky, I.A. Gudim, A.S. Krylov, A.V. Malakhovskii, V.L. Temerov, Upconversion luminescence of $YAl_3(BO_3)_4$:(Yb^{3+},Tm^{3+}) crystals, J. Alloys Compd. 496 (2010) L18–L21.
[6] Zhiguo Xia, Yuanyuan Zhang, Maxim S. Molokeev, Victor V. Atuchin, Structure and luminescence properties of yellow-emitting $NaScSi_2O_6$:Eu^{2+} phosphors: Eu^{2+} site preference analysis and generation of red emission by codoping Mn^{2+} for white-light-emitting diode applications, J. Phys. Chem. C 117 (2013) 20847–20854.
[7] V.V. Atuchin, O.D. Chimitova, S.V. Adichtchev, J.G. Bazarov, T.A. Gavrilova, M.S. Molokeev, N.V. Surovtsev, Zh.G. Bazarova, Syhtnesis, structural and vibrational properties of microcrystalline β-$RbSm(MoO_4)_2$, Mater. Lett. 106 (2013) 26–29.
[8] V.V. Atuchin, V.G. Kesler, A.I. Zaitsev, M.S. Molokeev, A.S. Aleksandrovsky, A.A. Kuzubov, N.Y. Ignatova, Electronic structure of α-SrB_4O_7: experiment and theory, J. Phys. Condens. Matter 25 (2013) 085503.
[9] Haipeng Ji, Zhaohui Huang, Zhiguo Xia, Maxim S. Molokeev, Victor V. Atuchin, Minghao Fang, Saifang Huang, New yellow-emitting whitlockite-type structure $Sr_{1.75}Ca_{1.25}(PO_4)_2$:$Eu^{2+}$ phosphor for near-UV pumped white light-emitting devices, Inorg. Chem. 53 (10) (2014) 5129–5135.
[10] Chang Sung Lim, Highly modulated structure and upconversion photoluminescence properties of $PbGd_2(MoO_4)_4$:Er^{3+}/Yb^{3+} phosphors, Mater. Res. Bull. 75 (2016) 211–216.
[11] V.V. Atuchin, V.G. Grossman, S.V. Adichtchev, N.V. Surovtsev, T.A. Gavrilova, B.G. Bazarov, Structural and vibrational properties of microcrystalline $TlM(MoO_4)_2$ (M = Nd, Pr) molybdates, Opt. Mater. 34 (5) (2012) 812–816.
[12] O.D. Chimitova, V.V. Atuchin, B.G. Bazarov, M.S. Molokeev, Z.G. Bazarova, The formation and structural parameters of new double molybdates $RbLn(MoO_4)_2$ (Ln = Pr, Nd, Sm, Eu), Proc. SPIE 8771 (2013) 87711A.
[13] Katrien W. Meert, Vladimir A. Morozov, Artem M. Abakumov, Joke Hadermann, Dirk Poelman, Philippe F. Smet, Energy transfer in Eu^{3+} doped scheelites: use as thermographic phosphor, Opt. Exp. 22 (S3) (2014) A961–A972.
[14] Wei Xie, Guixia Liu, Xiangting Dong, Jinxian Wang, Wensheng Yu, A direct warm-white-light $CaLa_2(MoO_4)_4$:Tb^{3+},Sm^{3+} phosphor with tunable color tone via energy transfer for white LEDs, RSC Adv. 5 (2015) 77866–77872.
[15] Chang Sung Lim, Upconversion photoluminescence properties of $PbY_2(MoO_4)_4$:Er^{3+}/Yb^{3+} phosphors synthesized by microwave sol-gel method, Bull. Korean Chem. Soc. 37 (4) (2016) 445–451.
[16] R.G. Teller, Refinement of some $Na_{0.5-x}M'_{0.5x+x/32x/3}MoO_4$, M′ = Bi, Ce, La, scheelite structures with powder neutron and X-ray diffraction data, Acta Cryst. C 48 (1992) 2101–2104.
[17] N.J. Stedman, A.K. Cheetham, P.D. Battle, Crystal structures of two sodium yttrium molybdates: $NaY(MoO_4)_2$ and $Na_5Y(MoO_4)_4$, J. Mater. Chem. 4 (5) (1994) 707–711.
[18] L. Macalik, Comparison of the spectroscopic and crystallographic data of Tm^{3+} in the different hosts: $KLn(MO_4)_2$ where Ln = Y, La, Lu and M = Mo, W, J. Alloys Compd. 341 (2002) 226–232.
[19] V.V. Atuchin, O.D. Chimitova, T.A. Gavrilova, M.S. Molokeev, Sung-Jin Kim, N.V. Surovtsev, B.G. Bazarov, Synthesis, structural and vibrational properties of microcrystalline $RbNd(MoO_4)_2$, J. Cryst. Growth 318 (2011) 683–686.
[20] Ying Li, Guofeng Wang, Kai Pan, Wei Zhou, Cheng Wang, Naiying Fan, Yajie Chen, Qingmao Feng, Binbin Zhao, Controlled synthesis and luminescence properties of rhombic $NaLn(MoO_4)_2$ submicrocrystals, CrystEngComm 14 (2012) 5015–5020.
[21] Jianfeng Tang, Yujin Chen, Yanfu Lin, Xinghong Gong, Jianhua Huang, Zundu Luo, Yidong Huang, Tm^{3+}/Ho^{3+} co-doped $LiGd(MoO_4)_2$ crystal as laser gain medium around 2.0 μm, Opt. Mater. Express 2 (8) (2012) 1064–1075.
[22] Pinglu Shi, Zhiguo Xia, Maxim S. Molokeev, Victor V. Atuchin, Crystal chemistry and luminescence properties of red-emitting $CsGd_{1-x}Eu_x(MoO_4)_2$ solid-solution phosphors, Dalton Trans. 43 (2014) 9669–9676.
[23] Chang Sung Lim, Fabrication and upconversion photoluminescence of $CaMoO_4$:Er^{3+},Yb^{3+} particles by a cyclic microwave-assisted metathetic method, Asian J. Chem. 24 (12) (2012) 5659–5661.
[24] Fangrui Cheng, Zhiguo Xia, Xiping Jing, Ziyuan Wang, Li/Ag ratio dependent structure and upconversion photoluminescence of $Li_xAg_{1-x}Yb_{0.99}(MoO_4)_2$: $0.01Er^{3+}$ phosphors, Phys. Chem. Chem. Phys. 17 (2015) 3689–3696.
[25] Chang Sung Lim, Aleksandr Aleksandrovsky, Maxim Molokeev, Aleksandr Oreshonkov, Victor Atuchin, The modulated structure and frequency upconversion properties of $CaLa_2(MoO_4)_4$:Ho^{3+}/Yb^{3+} phosphors prepared by microwave synthesis, Phys. Chem. Chem. Phys. 17 (2015) 19278–19287.
[26] R.K. Tamrakar, D.P. Bisen, K. Upadhyay, I.P. Sahu, Comparative study and role of Er^{3+} and Yb^{3+} concentrations on upconversion process of Gd_2O_3:$Er^{3+}Yb^{3+}$ phosphors prepared by solid-state reaction and combustion method, J. Phys. Chem. C 119 (36) (2015) 21072–21086.
[27] Chang Sung Lim, Preparation of $PbLa_2(MoO_4)_4$:Er^{3+}/Yb^{3+} particles via microwave sol-gel route and upconversion photoluminescence properties, Ceram. Int. 41 (2015) 12464–12470.
[28] Jia Zhang, Jianming Jia, Morphologies anfd up-conversion luminescence of $Gd_4O_3F_6$:RE^{3+} (RE = Yb, Er, Ho and Tm) phosphors by hydrothermal synthesis, J. Lumin 174 (2016) 1–5.
[29] J.P.C. do Nascimento, A.J.M. Sales, D.G. Sousa, M.A.S. da Silva, S.G.C. Moreira, K. Pavani, M.J. Soares, M.P.F. Graça, J. Suresh Kumar, A.S.B. Sombra, Temperature-, power-, and concentration-dependent two and three photon upconversion in Er^{3+}/Yb^{3+} co-doped lanthanum *ortho*-niobate phosphors, RSC Adv. 9 (72) (2016) 68160–68169.
[30] Chang Sung Lim, Microwave sol-gel derived $NaCaGd(MoO_4)_3$:Er^{3+}/Yb^{3+} phosphors and their upconversion photoluminescence properties, Inf. Phys. Technol. 76 (2016) 353–359.
[31] Chang Sung Lim, V.V. Atuchin, A.S. Aleksandrovsky, M.S. Molokeev, Preparation of $NaSrLa(WO_4)_3$:Ho^{3+}/Yb^{3+} ternary tungstates and their upconversion photoluminescence properties, Mater. Lett. 181 (2016) 38–41.
[32] K.I. Rybakov, E.A. Olevsky, E.V. Krikun, Microwave sintering: fundamentals and modeling, J. Am. Ceram. Soc. 96 (4) (2013) 1003–1020.
[33] H.J. Kitchen, S.R. Vallance, J.L. Kennedy, N. Tapia-Ruiz, L. Carassiti, A. Harrison, A.G. Whittaker, T.D. Drysdale, S.W. Kingman, D.H. Gregory, Modern microwave methods in solid-state inorganic materials chemistry: from fundamentals to manufacturing, Chem. Rev. 114 (2016) 1170–1206.
[34] Bruker AXS TOPAS V4: General Profile and Structure Analysis Software for Powder Diffraction Data. – User's Manual, Bruker AXS, Karlsruhe, Germany, 2008.
[35] R.M. Hazen, L.W. Finger, J.W.E. Mariathasan, High-pressure crystal chemistry of scheelite-type tungstates and molybdates, J. Phys. Chem. Solids 46 (1985) 253–263.
[36] S.B. Stevens, C.A. Morrison, T.H. Allik, A.L. Rheingold, B.S. Haggerty, $NaLa(MoO_4)_2$ as a laser host material, Phys. Rev. B 43 (1991) 7386–7394.
[37] I.C. Nogueira, L.S. Cavalcante, P.F.S. Pereira, M.M. De Jesus, J.M. Rivas Mercury, N.C. Batista, M.S. Li, E. Longo, Rietveld refinement, morphology and optical properties of $(Ba_{1-x}Sr_x)MoO_4$ crystals, J. Appl. Crystallogr. 46 (5) (2013) 1434–1446.
[38] B.G. Bazarov, R.F. Klevtsova, O.D. Chimitova, L.A. Glinskaya, K.N. Fedorov, Yu.L. Tushinova, Zh.G. Bazarova, Phase formation in the Rb_2MoO_4-$Er_2(MoO_4)_3$-$Hf(MO_4)_2$ system and the crystal structure of new triple molybdate $Rb_5ErHf(MoO_4)_6$, Russ. J. Inorg. Chem. 51 (5) (2006) 800–804.
[39] B.G. Bazarov, O.D. Chimitova, R.F. Klevtsova, Yu.L. Tushinova, L.A. Glinskaya, Zh.G. Bazarova, Crystal structure of a new ternary molybdate in the Rb_2MoO_4-$Eu_2(MoO_4)_3$-$Hf(MO_4)_2$ system, J. Struct. Chem. 49 (1) (2008) 53–57.
[40] V.V. Atuchin, T.A. Gavrilova, T.I. Grigorieva, N.V. Kuratieva, K.A. Okotrub, N.V. Pervukhina, N.V. Surovtsev, Sublimation growth and vibrational microspectrometry of α-MoO_3 single crystals, J. Cryst. Growth 318 (2011) 987–990.
[41] A.M. Abakumov, V.A. Morozov, A.A. Tsirlin, J. Verbeeck, J. Hadermann, Cation ordering and flexibility of the BO_4^{2-} tetrahedra in incommensurately modulated $CaEu_2(BO_4)_4$ (B = Mo, W) scheelites, Inorg. Chem. 53 (2014) 9407–9415.
[42] V.V. Atuchin, A.S. Aleksandrovsky, O.D. Chimitova, T.A. Gavrilova, A.S. Krylov, M.S. Molokeev, A.S. Oreshonkov, B.G. Bazarov, J.G. Bazarova, Synthesis and spectroscopic properties of monoclinic α-$Eu_2(MoO_4)_3$, J. Phys. Chem. C 118 (2014) 15404–15411.

[43] B. Greenberg, Polytechnic Institute of Brooklyn, ICDD Grant-in-Aid, Brooklyn, New York, USA, 1965.
[44] D. Saha, G. Madras, A.J. Bhattacharyya, T.N.G. Row, Synthesis, structure and ionic conductivity in scheelite type $Li_{0.5}Ce_{0.5-x}Ln_xMoO_4$ (x = 0 and 0.25, Ln = Pr, Sm), J. Chem. Sci. 123 (1) (2011) 5–13.
[45] U. Kolitsch, The crystal structures of phenacite-type $Li_2(MoO_4)$, and scheelite-type $LiY(MoO_4)_2$ and $LiNd(MoO_4)_2$, Z. Krist. 216 (8) (2001) 449–454.
[46] C.H. Chiu, M.F. Wang, C.S. Lee, T.M. Chen, Structural, spectroscopic and photoluminescence studies of $LiEu(WO_4)_{2-x}(MoO_4)_x$ as a near-UV convertible phosphor, J. Solid State Chem. 180 (2) (2007) 619–627.
[47] V.K. Rybakov, V.K. Trunov, About double molybdates of lithium and selected rare earth elements, Russ. J. Inorg. Chem. 14 (10) (1969) 2889–2980 (in Russian).
[48] M.C. McIlvried, Penn State University, University Park, Pennsylvania, USA, ICDD Grant-in-Aid (1973).
[49] V. Volkov, C. Cascales, A. Kling, C. Zaldo, Growth, structure, and evaluation of laser properties of $LiYb(MoO_4)_2$ single crystal, Chem. Mater. 17 (2) (2005) 291–300.
[50] T. Schleid, I. Hartenbach, Scheelite-type sodium neodymium (III) orthooxidomolybdate (VI), $NaNd[MoO_4]_2$, Acta Cryst. E 67 (12) (2011) i71.
[51] A. Arakcheeva, D. Logvinovich, G. Chapuis, V. Morozov, S.V. Eliseeva, J.C.G. Bünzli, P. Pattison, The luminescence of $Na_xEu^{3+}_{(2-x)/3}MoO_4$ scheelites depends on the number of Eu-clusters occurring in their incommensurately modulated structure, Chem. Sci. 3 (2) (2012) 384–390.
[52] G.M. Kuz'micheva, I.A. Kaurova, E.A. Zagorul'ko, N.B. Bolotina, V.B. Rybakov, A.A. Brykovskiy, E.V. Zharikov, D.A. Lis, K.A. Subbotin, Structural perfection of $(Na_{0.5}Gd_{0.5})MoO_4$: Yb laser crystals, Acta Mater. 87 (2015) 25–33.
[53] M.V. Savel'eva, I.V. Shakhno, V.E. Plyuschev, Synthesis and properties of molybdates of alkaline and selected rare earth elements, Inorg. Mater. 6 (9) (1970) 1665–1669 (in Russian).
[54] D. Zhao, F. Li, W. Cheng, H. Zhang, Scheelite-type $NaEr(MoO_4)_2$, Acta Cryst. E 66 (5) (2010) i36.
[55] V.B. Aleksandrov, L.V. Gorbatyii, V.V. Ilyukhin, Crystal structure of powellite $CaMoO_4$, Kristallografiya 13 (1968) 512–513.
[56] F. Shi, J. Meng, Y. Ren, Preparation, structure and some physical properties of scheelite-related $AgLnMo_2O_8$ compounds, J. Alloys Compd. 233 (1) (1996) 56–60.
[57] J. Meng, Chinese academy of sciences, Changchun, People's Republic of China, Priv. Commun. (1997).
[58] M. Rath, H. Müller-Buschbaum, Zur kristallstruktur von silber-lanthanoid-oxomolybdaten $AgLnMo_2O_8$: einkristalluntersuchungen an $AgSmMo_2O_8$ und $AgYbMo_2O_8$ mit einer notiz über mikrokristallines material für Ln= Y, La, J. Alloys Compd. 198 (1) (1993) 193–196.
[59] H.J. Zhang, L. Fu, C.P. Wang, H.F. Fu, W.G. Xie, Crystal structure of Scheelite-type potassium cerium bis (tetraoxomolybdate (VI)), $KCe(MoO_4)_2$, Z. Krist. 229 (3) (2014) 191–192.
[60] B.M. Wanklyn, F.R. Wondre, Flux growth of crystals of $RKMo_2O_8$, R_2MoO_6 and R_6MoO_{12} in the systems R_2O_3-K_2O-MoO_3, J. Cryst. Growth 43 (1) (1978) 93–100.
[61] A. Arakcheeva, P. Pattison, G. Chapuis, M. Rossell, A. Filaretov, V. Morozov, G. Van Tendeloo, $KSm(MoO_4)_2$, an incommensurately modulated and partially disordered scheelite-like structure, Acta Cryst. B 64 (2) (2008) 160–171.
[62] R.F. Klevtsova, L.P. Kozeeva, P.V. Klevtsov, Preparation and structure of crystals of potassium europium molybdate, $KEu(MoO_4)_2$, Kristallografiya 19 (1974) 89–94.
[63] B. Lazoryak, X-ray Powder Diffraction Laboratory of Chemistry Technology, Moscow State Univ., Russia, ICDD Grant-in-Aid, 1999.
[64] V.A. Morozov, A.V. Mironov, B.I. Lazoryak, E.G. Khaikina, O.M. Basovich, M.D. Rossell, G. Van Tendeloo, $Ag_{1/8}Pr_{5/8}MoO_4$: an incommensurately modulated scheelite-type structure, J. Solid State Chem. 179 (4) (2006) 1183–1191.
[65] V.A. Morozov, A.V. Arakcheeva, B.S. Redkin, V.V. Sinitsyn, S.S. Khasanov, E.V. Kudrenko, M.V. Raskina, O.I. Lebedev, G. Van Tendeloo, $Na_{2/7}Gd_{4/7}MoO_4$: a modulated scheelite-type structure and conductivity properties, Inorg. Chem. 51 (2012) 5313–5324.
[66] V.A. Morozov, B.I. Lazoryak, S.Z. Shmurak, A.P. Kiselev, O.I. Lebedev, N. Gauquelin, J. Verbeek, J. Hadermann, G. Van Tendeloo, Influence of the structure on the properties of $Na_xEu_y(MoO_4)_z$ red phosphors, Chem. Mater. 26 (10) (2014) 3238–3248.
[67] R.D. Shennon, Revised effective ionic radii and systematic studies of interatomic distances in halides and chalcogenides, Acta Cryst. A 32 (1876) 751–767.
[68] V.V. Atuchin, T.A. Gavrilova, J.-C. Grivel, V.G. Kesler, Electronic structure of layered titanate $Nd_2Ti_2O_7$, Surf. Sci. 602 (2008) 3095–3099.
[69] V.V. Atuchin, B.G. Bazarov, T.A. Gavrilova, V.G. Grossman, M.S. Molokeev, Zh.G. Bazarova, Preparation and structural properties of nonlinear optical borates $K_{2(1-x)}Rb_{2x}Al_2B_2O_7$, $0<x<0.75$, J. Alloys Compd. 515 (2012) 119–122.
[70] Chang Sung Lim, A.S. Aleksandrovsky, M.S. Molokeev, A.S. Oreshonkov, D.A. Ikonnikov, V.V. Atuchin, Triple molybdate scheelite-type upconversion phosphor $NaCaLa(MoO_4)_3$:Er^{3+}/Yb^{3+}: structural and spectroscopic properties, Dalton Trans. 45 (2016) 15541–15551.
[71] M.B. Smirnov, V. Yu. Kazimirov, JINR Commun. E (2001), 14-2001-159.
[72] A.S. Krylov, M.S. Molokeev, S.V. Misyul, S.N. Krylova, A.S. Oreshonkov, A.A. Ivanenko, V.A. Zykova, Y.N. Ivanov, A.A. Sukhovsky, V.N. Voronov, I.N. Safonov, A.N. Vtyurin, Crystal structure and phase transitions of a layered perovskite-like $CsScF_4$ crystal, CrystEngComm 18 (2016) 8472–8486.
[73] E.A. Strikina, A.S. Krylov, A.S. Oreshonkov, A.N. Vtyurin, Raman scattering study of δ-BiB_3O_6 crystal, Ferroelectrics 501 (1) (2016) 26–31.
[74] A.S. Oreshonkov, A.S. Krylov, N.P. Shestakov, V.N. Voronov, A.A. Ershov, E.A. Strikina, A.N. Vtyurin, Vibrational spectra of NdF_3 crystal, Ferroelectrics 501 (1) (2016) 15–19.
[75] C.S. Lim, V.V. Atuchin, A.S. Aleksandrovsky, M.S. Molokeev, A.S. Oreshonkov, Incommensurately modulated structure and spectroscopic properties of $CaGd_2(MoO_4)_4$:Ho^{3+}/Yb^{3+} phosphors for up-conversion applications, J. Alloys Compd. (2016), http://dx.doi.org/10.1016/j.jallcom.2016.06.134.
[76] A.S. Oreshonkov, J.V. Gerasimova, A.A. Ershov, A.S. Krylov, K.A. Shaykhutdinov, A.N. Vtyurin, M.S. Molokeev, K.Y. Terent'ev, N.V. Mihashenok, Raman spectra and phase composition of $MnGeO_3$ crystals, J. Raman Spectrosc. 47 (5) (2016) 531–536.
[77] Yu.V. Gerasimova, S.N. Sofronova, I.A. Gudim, A.S. Oreshonkov, A.N. Vtyurin, A.A. Ivanenko, Infrared absorption spectra of a $Nd_{0.5}Ho_{0.5}Fe_3(BO_3)_4$ crystal, Phys. Solid State 58 (1) (2016) 155–159.
[78] C.S. Lim, A. Aleksandrovsky, M. Molokeev, A. Oreshonkov, V. Atuchin, Microwave sol–gel synthesis and upconversion photoluminescence properties of $CaGd_2(WO_4)_4$:Er^{3+}/Yb^{3+} phosphors with incommensurately modulated structure, J. Solid State Chem. 228 (2015) 160–166.
[79] A.A. Savina, V.V. Atuchin, S.F. Solodovnikov, Z.A. Solodovnikova, A.S. Krylov, E.A. Maximovskiy, M.S. Molokeev, A.S. Oreshonkov, A.M. Pugachev, E.G. Khaikina, Synthesis, structural and spectroscopic properties of acentric triple molybdate $Cs_2NaBi(MoO_4)_3$, J. Solid State Chem. 225 (2015) 53–58.
[80] Zhiguo Xia, M.S. Molokeev, A.S. Oreshonkov, V.V. Atuchin, Ru-Shi Liu, Cheng Dong, Crystal and local structure refinement in $Ca_2Al_3O_6F$ explored by X-ray diffraction and Raman spectroscopy, Phys. Chem. Chem. Phys. 16 (2014) 5952–5957.
[81] Y.V. Gerasimova, A.S. Oreshonkov, A.N. Vtyurin, A.A. Ivanenko, L.I. Isaenko, A.A. Ershov, E.I. Pogoreltsev, Imfrared absorption investigation of the role of octahedral groups upon the phase transition in the $Rb_2KMoO_3F_3$ crystal, Phys. Solid State 55 (11) (2013) 2331–2334.
[82] A.S. Krylov, A.N. Vtyurin, A.S. Oreshonkov, V.N. Voronov, S.N. Krylova, Structural transformations in single crystal Rb_2NaYF_6: Raman scattering study, J. Raman Spectr. 44 (5) (2013) 763–769.
[83] A.N. Vtyurin, A.S. Krylov, S.N. Krylova, S.V. Goryainov, V.N. Voronov, A.S. Oreshonkov, Hydrostatic pressure-induced phase transitions in Rb_2KInF_6 and Rb_2KScF_6 crystals: Raman spectra and lattice dynamics simulations, Ferroelectrics 440 (2012) 100–104.
[84] A.N. Vtyurin, A.S. Krylov, S.V. Goryainov, S.N. Krylova, A.S. Oreshonkov, V.N. Voronov, A Raman study of hydrostatic pressure induced phase transitions in Rb_2KInF_6 crystals, Phys. Solid State 54 (5) (2012) 934–936.
[85] K. Nakamoto, Infrared and Raman Spectra of Inorganic and Coordination Compounds, sixth ed., Wiley, New York etc, 2009.
[86] J. Hanuza, M. Maczka, Vibrational properties of the double molybdates $MX(MoO_4)_2$ family (M = Li,Na, K,Cs; X = Bi,Cr) Part I. Structure and infrared and Raman spectra in the polycrystalline state, Vib. Spectrosc. 7 (1994) 85–96.
[87] J. Hanuza, M. Maczka, J.H. van der Maas, Polarized IR and Raman spectra of tetragonal $NaBi(WO_4)_2$, $NaBi(MoO_4)_2$ and $LiBi(MoO_4)_2$ single crystals with scheelite structure, J. Mol. Struct. 348 (1995) 349–352.